Direct numerical simulation of forced thermal convection in square ducts

Modesti, Davide; Pirozzoli, Sergio

12th International Symposium on Turbulence and Shear Flow Phenomena (TSFP12)
Osaka, Japan (Online), July 19-22, 2022

DIRECT NUMERICAL SIMULATION OF FORCED THERMAL CONVECTION IN SQUARE DUCTS

Davide Modesti
Faculty of Aerospace Engineering
Delft University of Technology
Kluyverweg 2, 2629 HS Delft, The Netherlands
d.modesti@tudelft.nl

Sergio Pirozzoli
Dipartimento di Ingegneria Meccanica e Aerospaziale
Sapienza Università di Roma
via Eudossiana 18, 00184 Roma, Italia
sergio.pirozzoli@uniroma1.it

ABSTRACT

We carry out direct numerical simulation (DNS) of flow in a turbulent square duct by focusing on heat transfer effects, considering the case of unit Prandtl number. Reynolds numbers up to $Re_\tau \approx 2000$ are considered which are much higher than in previous studies, and which yield clear scale separation between inner- and outer-layer dynamics. Close similarity between the behavior of the temperature and the streamwise velocity fields is confirmed as in previous studies related to plane channels and pipes. We find good agreement between the Nusselt number of square duct and circular pipe flow when the Reynolds number based on the hydraulic diameter is used, thus corroborating the common engineering practice. Popular engineering correlations for the heat transfer reveal deviations up to 5% with respect to DNS data, which are nicely fitted by a power law.

INTRODUCTION

Heat transfer in internal flows is a subject of utmost relevance in mechanical and aerospace engineering applications. A large amount of experimental and numerical studies have been carried out in the past, and a variety of analytical and semi-empirical prediction tools have been developed, which are extensively reported in classical textbooks (Kays & Crawford, 1993). Most studies have been carried out for the canonical case of ducts with circular cross section, whereas much less is known about the case of ducts with more complex geometry, which also have great practical relevance, for instance in water draining or ventilation systems, nuclear reactors, heat exchangers, space rockets and turbomachinery.

In that case, the typical engineering approach is to use the same correlations established for the case of circular pipes, by replacing the pipe diameter with the hydraulic diameter of the duct (Kays & Crawford, 1993). However, the large scatter in experimental data makes it difficult to quantify the actual accuracy of semi-empirical prediction formulas.

Heat transfer in square ducts was first studied experimentally by Brundrett & Burroughs (1967), who considered air flow at bulk Reynolds number $Re_b = Hu_b/\nu$ (where $H = 2h$ is duct side length and also duct hydraulic diameter, u_b is the bulk velocity, and ν the fluid kinematic viscosity) 33000 and 67000. Close similarity between the wall shear stress and the heat flux distributions was shown (with quoted discrepancy of $\pm 2\%$), which the authors connected with similar mixing action of the secondary currents on momentum and temperature. As a result, they observed that the ratio of the average friction and heat-transfer coefficients for a square duct is approximately the same as for a circular pipe. Measurements of the wall-normal temperature profiles highlighted close universality when the local wall heat flux is used for normalization, and the presence of a sizeable logarithmic layer, with extrapolated value of the scalar Kármán constant of $\kappa_\theta \approx 0.51$. Those findings were qualitatively supported from later experiments by Hirota *et al.* (1997), who also analysed temperature fluctuations and velocity/temperature fluctuations correlations, and found significant distortions over the cross section associated with the secondary motions. In that study, the inferred scalar von Kármán constant was $\kappa_\theta \approx 0.46$, hence more similar to the values generally quoted for circular pipe flow, namely $\kappa_\theta \approx 0.47$ (Kader & Yaglom, 1972).

Early computational studies of heat transfer in square ducts mostly relied on the use of RANS models (Launder & Ying, 1973), but heat transfer coefficient showed general underprediction by about 10%. High-fidelity computational studies of heat transfer in square ducts have been quite limited so far. Vázquez & Métais (2002) first studied turbulent flow through a heated square duct by means of large-eddy simulation (LES) at bulk Reynolds number $Re_b = 6000$, considering the case in which one of the walls is hotter than the other three. Accounting for fluid viscosity variation with temperature, they found that turbulent structures near the hot wall become larger than near the other walls, in such a way that wall scaling is satisfied.

In this paper we study heat transfer in fully developed square duct flow with uniform internal heating and isothermal walls, by carrying out DNS at unit molecular Prandtl number (defined as the ratio of the kinematic viscosity to the scalar diffusivity, $Pr = \nu/\alpha$), and at much higher Reynolds number than in previous computational studies, The present study

Table 1. Flow parameters for square duct DNS. Box dimensions are $6\pi h \times 2h \times 2h$ for all flow cases. $Re_b = 2hu_b/\nu$ is the bulk Reynolds number, $Re_\tau^* = hu_\tau^*/\nu$ is the friction Reynolds number, and Nu is the Nusselt number. $N_x \times N_y \times N_z$ are the mesh points in the respective coordinate directions.

Case	Re_b	Re_τ^*	Nu	N_x	N_y	N_z
A	4410	150	18.1	512	128	128
B	7000	227	26.9	640	144	144
C	12000	365	41.9	768	208	208
D	17800	519	57.6	1024	256	256
E	40000	1055	109.0	2048	512	512
F	84000	2041	197.0	4096	1024	1024

is the continuation of previous efforts (Pirozzoli *et al.*, 2018; Modesti *et al.*, 2018) targeted to studying turbulent flows in square ducts by means of DNS.

1 METHODOLOGY

In the present work we use a fourth-order co-located finite-difference solver, previously used for DNS of compressible turbulence (Bernardini *et al.*, 2021). Here, semi-implicit time stepping is used for time advancement in order to relax the acoustic time step limitation, thus allowing efficient operation at low Mach number (Modesti & Pirozzoli, 2018). The streamwise momentum equation is forced in such a way as to maintain a constant mass flow rate (the spatially uniform driving term is hereafter referred to as Π), periodicity is exploited in the streamwise direction, and isothermal no-slip boundary conditions are used at the channel walls. Six DNS have been carried out at bulk Mach number $M_b = u_b/c_w = 0.2$ (where c_w is the speed of sound at the wall temperature), and bulk Reynolds number $Re_b = 4400 - 84000$ (table 1), and hereafter labeled with letters from A to F. Navier–Stokes equations are augmented with the transport equation for a passive scalar field, with molecular diffusivity $\alpha = \nu$, in such a way that the molecular Prandtl number is unity for all simulations. Similarly to the streamwise velocity field, the passive scalar equation is also forced with a time-varying, spatially homogeneous forcing term Q, in such a way that its mean value is maintained in time.

The $+$ superscript is used to denote quantities made nondimensional with respect to the local wall friction, namely with $u_\tau = (\tau_w/\rho)^{1/2}$ ($\tau_w = \nu dU/dy|_w$ is the local wall shear stress), and $\delta_\nu = \nu/u_\tau$, and the $*$ superscript is used to denote quantities made nondimensional with respect to the perimeter-averaged friction, $\tau_w^* = h\langle\Pi\rangle/2$, namely $u_\tau^* = (\tau_w^*/\rho)^{1/2}$, and $\delta_\nu^* = \nu/u_\tau^*$. Likewise, for normalization of the temperature field we will consider either the local friction temperature $\theta_\tau = q_w/u_\tau$, where $q_w = \alpha d\Theta/dy|_w$ is the local wall heat flux, or the global friction temperature θ_τ^*.

RESULTS

We begin by inspecting the instantaneous streamwise velocity and temperature fields in figure 1, which shows the flow both in the cross-stream and wall-parallel planes. Instantaneous flow structure are not different from the ones typical of canonical wall flows, and the near wall of both temperature and streamwise velocity is populated with streaks, resulting from sweep and ejections visible in the cross-stream plane. In the cross-stream plane we note bulges of high-speed and hot flow spanning two opposite walls, and interacting with the smaller structures close to the wall. We immediately note a strong similarity between streamwise velocity and temperature, with the main difference that the latter reveals much finer structures due to the absence of the smoothing action of the pressure gradient. The picture that emerges from the instantaneous snapshots is similar to the one of other canonical wall flows, instead, the mean flow field is characterized by the presence of secondary flows in the cross-stream plane.

Figure 2 depicts the mean temperature (contours) and velocity (iso-lines) fields in the duct cross section, along with representative cross-stream velocity vectors. This representation brings to light the presence of a pair of counter-rotating secondary eddies in each quarter of the domain, whose apparent role is bringing high-speed, and high-temperature fluid from the duct core towards the corners, which are relatively depleted with those. As a result, both the temperature contours and the velocity isolines bend towards the corners, featuring a bulging first noticed by Nikuradse (1930). This effect seems to be non-monotonic with the Reynolds number, being most evident for DNS-A and DNS-E/F. As expected, temperature and velocity contours bear close similarity, being nearly coincident near the wall, and retaining the same shape farther off.

Figure 3 shows the mean temperature profiles as a function of the wall-normal distance up to the corner bisector (white dashed line in figure 2), in global wall units (based on the perimeter-averaged wall-shear stress). For reference purposes, the mean temperature profiles obtained with the experimental fitting by Kader (1981) at matching Re_τ are also reported. Scatter among the temperature profiles is observed near the wall as a result of the local variation of the wall heat flux. Perhaps unexpectedly, this normalization yields good universality away from walls, and near coincidence with the pipe temperature profiles, at least at high enough Reynolds number. This finding is probably related to the fact that mean temperature transport away from solid walls is controlled by the imposed spatially uniform heat source rather than by the nonuniform wall heat flux. Inspection of figure 3 shows that transition to the 'global' scaling (which is controlled by the spatially uniform heat source) occurs at a wall distance of about $0.2h$, which is also the lower limit for the core region in canonical flows (Pope, 2000). These results support findings previously reported for the streamwise velocity (Pirozzoli *et al.*, 2018), and confirm that square duct flow is a convenient testbed for evaluating differences between local and global scaling.

The global heat transfer performance of the duct is quantified in terms of the Stanton number, $St^* = 1/(u_b^*\theta_m^*)$, where u_b and θ_m are the bulk flow velocity and bulk temperature temperature,

$$\theta_m = \frac{1}{u_b A_c}\int_{A_c} U(\Theta - \theta_w)dA_c, \quad u_b = \frac{1}{A_c}\int_{A_c} U dA_c. \quad (1)$$

Additionally, we also quantify the heat transfer using the Nusselt number, $Nu^* = St^* Re_b Pr$.

In figure 4 we compare the distributions of the heat transfer coefficients (inverse Stanton number and Nusselt number) obtained from the present DNS (squares) with those resulting from DNS of circular pipe flow (circles), from previous LES (diamonds), and from experiments (triangles) in square

ducts. We note that the latter two datasets were obtained for $Pr = 0.71$, hence the Nu data have been rescaled by a factor $1/\sqrt{Pr}$ to compare with the present ones. As a reference, we also report correlations widely used in the engineering practice, including that by Gnielinski (1976), from Kays & Crawford (1993) and direct fitting the present DNS data with a power-law expression which yields, $Nu = 0.0216 Re_b^{0.805}$. The DNS data show good correspondence with the pipe DNS data at matching Re_b, with the exception of the lower Reynolds number case, which supports validity of the hydraulic diameter concept as the relevant length scale for heat transfer data reduction. Agreement with experiments and LES in square ducts is also quite good, on account of experimental uncertainties and modeling errors in LES. It is interesting that differences are levelled off when the popular representation in terms of the Nusselt number is used, as in figure 4(b), hence we believe that the $1/St$ representation should be used when relatively small differences must be discriminated. Classical correlations seem to suggest systematic difference of up to 5% in the prediction of the heat transfer coefficient. This difference may be partly due to inaccuracy of correlations based on old experimental data, or to the fact that those are mainly trained for the $Pr = 0.71$ case, whereas here $Pr = 1$. Additionally, discrepancies can be attributed to our heat forcing scheme, in which a spatially uniform heat source is prescribed, which tends to slightly overpredict the heat flux as compared to other approached in which the total heat flux is kept strictly constant in time (Abe & Antonia, 2017). Slight adjustment of the Kays–Crawford power-law formula coefficients seems to yield very good representation of the DNS data.

An issue which deserves further investigation is why use of the hydraulic diameter yields excellent results, at least in the case of square ducts under consideration. Pirozzoli *et al.* (2018) showed that universality of friction is connected with near applicability of the logarithmic velocity law in the direction normal to the nearest wall. It is worthwhile verifying whether it is also the case of the heat flux coefficient. As previously shown, the temperature distributions are nearly universal away from walls, even when expressed in global wall units. Hence, approximating the outer layer profiles with the classical log law, namely $U^* = 1/\kappa \log y^* + C$, $\Theta^* = 1/\kappa_\theta \log y^* + C_\theta$, and integrating over the duct cross section, the following expression for the inverse Stanton number results

$$\begin{aligned} 1/St^* = \frac{8}{4Re_\tau^{*2}} \int_0^h \int_0^z \left[\frac{1}{\kappa\kappa_\theta} \log y^{*2} \right. \\ \left. + \log y^* \left(\frac{C_\theta}{\kappa} + \frac{C}{\kappa_\theta} \right) + CC_\theta \right] dy^* dz^* = \\ \frac{1}{\kappa\kappa_\theta} \left(\log^2 Re_\tau^* + 3 \log Re_\tau^* + \frac{7}{2} \right) \\ + \left(\frac{C_\theta}{\kappa} + \frac{C}{\kappa_\theta} \right) \left(\log Re_\tau^* - \frac{3}{2} \right) + CC_\theta . \end{aligned} \tag{2}$$

Equation (2) should be compared with the corresponding expression for a circular duct with diameter D,

$$\begin{aligned} 1/St = \frac{1}{\kappa\kappa_\theta} \left(\log^2 Re_\tau + 3 \log Re_\tau + \frac{7}{2} \right) \\ + \left(\frac{C_\theta}{\kappa} + \frac{C}{\kappa_\theta} \right) \left(\log Re_\tau - \frac{3}{2} \right) + CC_\theta , \end{aligned} \tag{3}$$

where $Re_\tau = Du_\tau/(2\nu)$. The two expressions are identical for $2h = D$, hence provided the Reynolds number based on the hydraulic diameter is the same. It is interesting that equation (2) is basically arrived at by neglecting the local wall shear stress and heat flux variation along the duct perimeter, and disregarding the flow deceleration at corners. Apparently, these effects very nearly cancel out upon integration.

CONCLUSIONS AND FUTURE WORK

We have carried out DNS of square duct flow at the unprecedented Reynolds number of $Re_\tau \approx 2000$, wherein Navier–Stokes equations have been augmented with the transport of a passive scalar representing the temperature field. This configuration corresponds to the case of forced convection in which hot fluid is pumped through the duct and cooled at the walls. In this respect, we find that the streamwise velocity and temperature fields are very similar, both instantaneously and on average.

The Nusselt number of square duct flow is in excellent agreement with pipe flow data at matching Reynolds number, which support the validity of the hydraulic diameter concept. We explain this good match by using a simple model in which the duct flow can be regarded as the superposition of four concurrent walls, where the flow is controlled by the closest one. This simple cartoon is well supported by the mean temperature profiles in a duct octant, which follow with good accuracy the canonical law-of-the-wall. An extensive analysis of this DNS dataset is available in our recent publication (Modesti & Pirozzoli, 2022), where we also discuss the temperature fluctuations and the accuracy of eddy viscosity models for the turbulent heat transfer. Future effort will be devote to study the flow in asymmetrically heated square and rectangular ducts, which is a common configuration in heat exchangers.

REFERENCES

Abe, H. & Antonia, R.A. 2017 Relationship between the heat transfer law and the scalar dissipation function in a turbulent channel flow. *J. Fluid Mech.* **830**, 300–325.

Bernardini, M., Modesti, D., Salvadore, F. & Pirozzoli, S. 2021 STREAmS: A high-fidelity accelerated solver for direct numerical simulation of compressible turbulent flows. *Comput. Phys. Commun.* **263**, 107906.

Brundrett, E. & Burroughs, P.R. 1967 The temperature inner-law and heat transfer for turbulent air flow in a vertical square duct. *Int. J. Heat Mass Transfer* **10**, 1133–1142.

Gnielinski, V. 1976 New equations for heat and mass transfer in turbulent pipe and channel flow. *Int. Chem. Eng.* **16**, 359–367.

Hirota, M., Fujita, H., Yokosawa, H., Nakai, H. & Itoh, H. 1997 Turbulent heat transfer in a square duct. *Int. J. Heat Fluid Flow* **18**, 170–180.

Kader, B.A. 1981 Temperature and concentration profiles in fully turbulent boundary layers. *Int. J. Heat Mass Transf.* **24** (9), 1541–1544.

Kader, B.A. & Yaglom, A.M. 1972 Heat and mass transfer laws for fully turbulent wall flows. *Int. J. Heat Mass Trans.* **15** (12), 2329–2351.

Kays, W.M. & Crawford, M.E. 1993 Convective heat and mass transfer, 3rd edn.

Launder, B.E. & Ying, W.M. 1973 Prediction of flow and heat transfer in ducts of square cross-section. *Proc. Instn. Mech. Engrs.* **187** (1), 455–461.

Modesti, D. & Pirozzoli, S. 2018 An efficient semi-implicit solver for direct numerical simulation of compressible flows at all speeds. *J. Sci. Comput.* **75** (1), 308–331.

Modesti, D. & Pirozzoli, S. 2022 Direct numerical simulation of forced thermal convection in square ducts up to $\mathrm{Re}_\tau \approx 2000$. *J. Fluid Mech.* **941**, A16.

Modesti, D., Pirozzoli, S., Orlandi, P. & Grasso, F. 2018 On the role of secondary motions in turbulent square duct flow. *J. Fluid Mech.* **847**.

Nikuradse, J. 1930 Turbulente strömung in nicht-kreisförmigen rohren. *Ing. Arch.* **1**, 306–332.

Pallares, J. & Davidson, L. 2002 Large-eddy simulations of turbulent heat transfer in stationary and rotating square ducts. *Phys. Fluids* **14** (8), 2804–2816.

Pirozzoli, S., Modesti, D., Orlandi, P. & Grasso, F. 2018 Turbulence and secondary motions in square duct flow. *J. Fluid Mech.* **840**, 631–655.

Pirozzoli, S., Romero, J., Fatica, M., Verzicco, R. & Orlandi, P. 2021 One-point statistics for turbulent pipe flow up to $\mathrm{Re}_\tau \approx 6000$. *J. Fluid Mech.* **926**, A28.

Pope, S.B. 2000 *Turbulent flows*. Cambridge University Press.

Vázquez, M.S. & Métais, O. 2002 Large-eddy simulation of the turbulent flow through a heated square duct. *J. Fluid Mech.* **453**, 201–238.

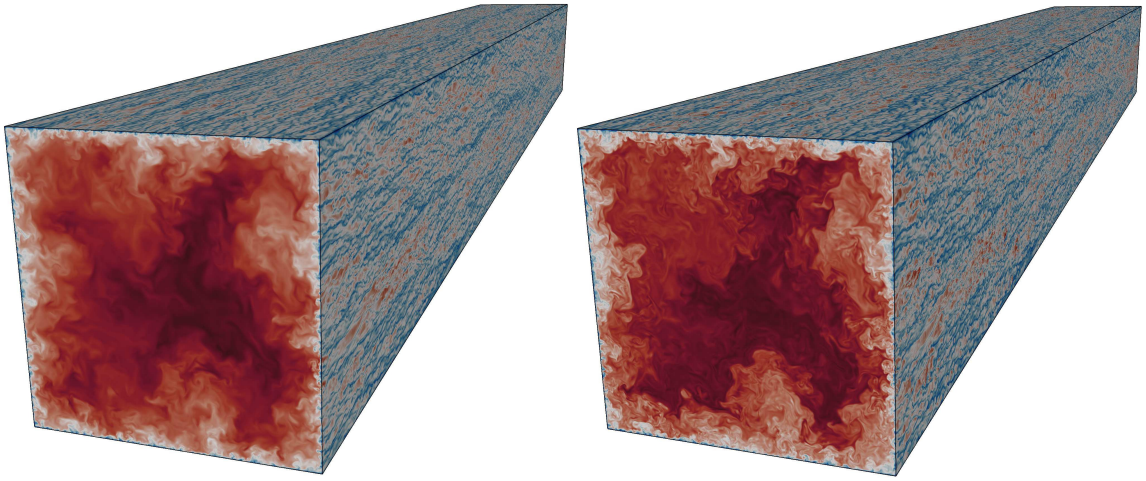

Figure 1. Instantaneous streamwise velocity (*a*) and temperature (*b*) fields for flow case F. Wall-parallel planes are taken 15 wall units from the walls.

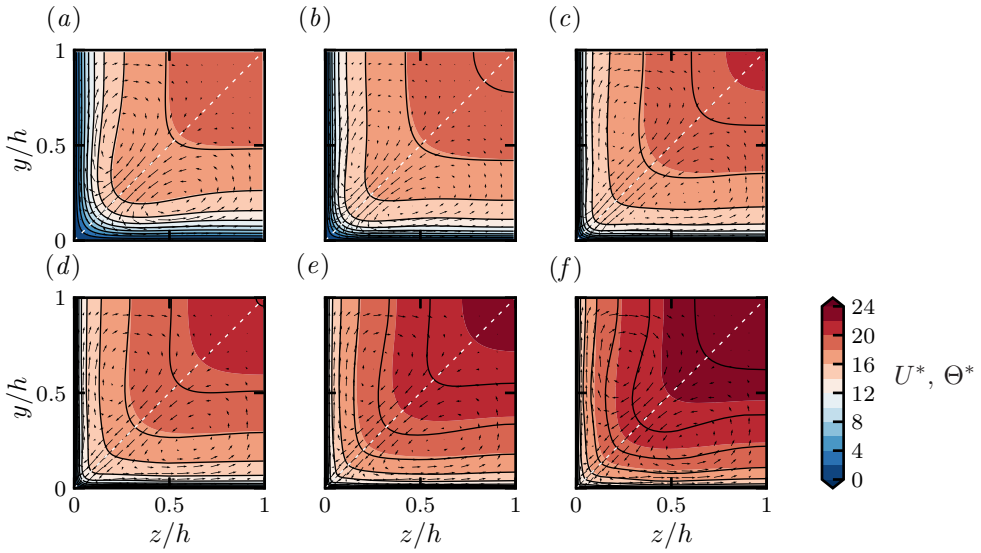

Figure 2. Mean streamwise temperature (Θ^*, flooded contours), mean streamwise velocity (U^*, lines), and mean cross-stream velocity vectors (V^*, W^*) for flow cases A (*a*), b (*b*), C (*c*), D (*d*), E (*e*), F (*f*). For clarity, only a subset of the velocity vectors are shown. Only a quarter of the full domain is shown. The dashed diagonal lines indicate the corner bisector.

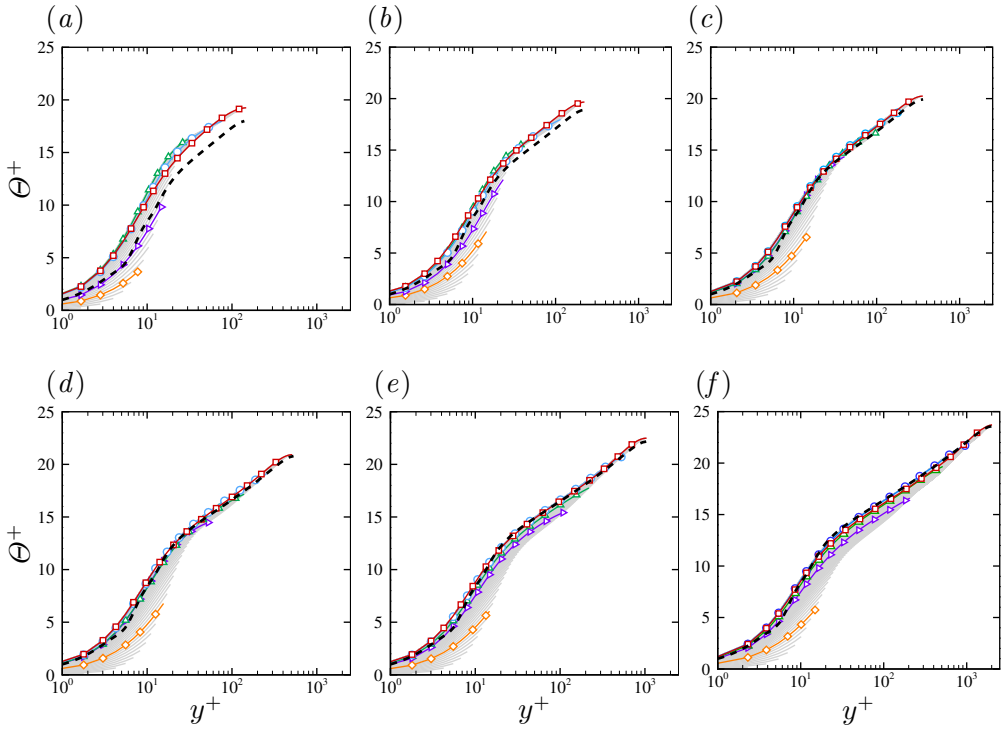

Figure 3. Mean wall-normal temperature profiles scaled in global wall units for flow cases A (*a*), B (*b*), C (*c*), D (*d*), E (*e*), F (*f*). Profiles are plotted at several distances from the left wall, up to the corner bisector (see figure 2 for reference): $z^* = 15$ (diamonds), $z/h = 0.1$ (right triangles), $z/h = 0.25$ (triangles), $z/h = 0.5$ (circles), $z/h = 1$ (squares). The dashed lines denote fit of experimental data (Kader, 1981), at matching Re_τ^*.

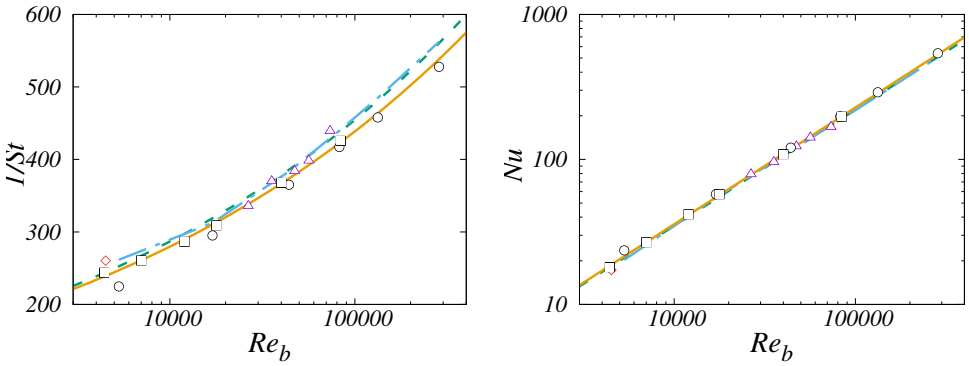

Figure 4. Inverse Stanton number (a) and Nusselt number (b) as a function of bulk Reynolds number, from the present DNS (squares), from DNS of circular pipe flow (circles Pirozzoli *et al.*, 2021), from previous LES (diamonds Pallares & Davidson, 2002), and from experiments (Brundrett & Burroughs, 1967, triangles). The dashed line denotes the correlation by Kays & Crawford (1993), and the dot-dashed lines the correlation Gnielinski (1976).